European Congress on Computational Methods
in Applied Sciences and Engineering (ECCOMAS 2012)
J. Eberhardsteiner et.al. (eds.)
Vienna, Austria, September 10-14, 2012

ELASTO-HYDRODYNAMIC LUBRICATION OF ROUGH CONTACTS: ON A RIGOROUS GENERALISATION OF THE HOMOGENISATION APPROACH

Bernhard Scheichl[1,2] **and Francesco S. Guerrieri Paleotti**[1,3]

[1] AC²T research GmbH (Austrian Center of Competence for Tribology)
Viktor-Kaplan-Straße 2D, A-2700 Wiener Neustadt, Austria
e-mail: {scheichl,guerrieri}@ac2t.at

[2] Vienna University of Technology, Institute of Fluid Mechanics and Heat Transfer
Resselgasse 3/E322, A-1040 Vienna, Austria
e-mail: bernhard.scheichl@tuwien.ac.at

[3] University of Pisa, Department of Mechanical, Nuclear, and Production Engineering
Via Diotisalvi 2, 56100 Pisa, Italy
e-mail: f.guerrieri@amtesting.net

Keywords: elasto-hydrodynamics, homogenisation methods, surface roughness, tribology

Abstract. *The rigorous theory of elasto-hydrodynamic lubrication of rough contacts based on homogenisation techniques is extended with the aim to include (i) the presence of not only wetted but also isolated dry contact regions, (ii) the deformation of the single asperity spikes, and (iii) periodic or even quasi-periodic roughness patterns involving several scales. The typical asymptotic two-scale approach proves sufficient to cope with these effects, but the complexity of the problem is considerably increased. Aspect (i) essentially affects the central homogenised problem as free boundaries separate the dry islands from the lubrication gap, filled with liquid/cavitating lubricant. Issue (ii) introduces a further coupling between the scales as it modifies the lowest-order problem governing the small-scale variation of the contact pressure due to roughness. The generalisation addressed by (iii) requires a non-standard averaging as a large-scale modulation of the roughness waviness is considered. The homogenised quantities are advantageously non-dimensional with the semi-axes of the contact ellipse and the reference pressure of Hertzian contact. Specific emphasis is laid on the behaviour of the system relatively far from the associated contact ellipse and the limiting case of relatively high loads (i.e. that close to purely Hertzian conditions), so as to answer the long-standing fundamental question of the average thickness of the very thin liquid film separating the contacts in a rational manner. A numerical case study accompanies the analysis.*

1 INTRODUCTION

Our concern is with the local formulation of a general tribological contact problem, i.e. two elastic half-spaces having paraboloidal shapes and separated (non-conformally) by a lubricated gap and/or in dry contact due to the action of an external load. If the mean height of the surface asperities of the solid paraboloids is small compared to their elastic deformations and the clearance height, if these two quantities are small compared to a characteristic diameter of a dry contact area, if this in turn is small compared to the typical curvature radii of the paraboloids, and if inertia and thermal effects have insignificant effect on the dynamics of the incompressible Newtonian lubricant, the contact pressure is described by classical elasto-hydrodynamic lubrication (EHL) theory to leading order. Here the aforementioned small ratios serve as the principal perturbation parameters that give rise to an asymptotic theory. In the conventional formulation of this theory, see e.g. [1], dry regions or so-called starved lubrication are excluded. A more challenging (though more realistic from an engineering point of view) situation arises if this and the first of the above assumption are relaxed, leading to so-called mixed lubrication. Then the points (i)–(iii) raised in the Abstract come into play, requiring a careful revision of the classical analysis. Most important, this ceases to be valid when the gap height and the mean amplitude of the roughness elements are assumed to be of the same order of magnitude, whereas the wavelengths introduced by the latter are typically much smaller.

Apart from the issues (i)–(iii), in this contribution the main focus lies on a most comprehensive formulation of the EHL problem. Specific attention is paid to the behaviour of the pressure and the elastic deflections on the one hand relatively far from the region of immediate contact and, on the other hand, or under relatively high loads. The insight gained analytically feeds into a novel numerical computational scheme we believe to efficiently cope with the intriguing but challenging case of highly loaded contacts separated by a very thin lubricant film.

2 FORMULATION OF THE GENERAL PROBLEM

On the large or macroscopic scale, measured by the axes of the Hertzian contact ellipse associated with the case of purely dry contact, the problem described in a frame of reference fixed to the plane tangential to both paraboloid solid bodies I and II and their sliding motion relative to the reference frame (and often to one of those), is taken as stationary. For what follows, in any physical quantity referring to one of the contact bodies this is identified by an index. The geometrical situation under nearly Hertzian conditions, generating an elliptic flattening of the bodies, is sketched in figure 1. Let $\boldsymbol{x} = (x_1, x_2)$ denote Cartesian coordinates aligned with that tangential plane and the principal directions of the resultant paraboloid representing the gap and thus with the semi-axes $\tilde{a}$ and $\tilde{b}$ of the Hertzian contact ellipse, respectively, where we assume that $\tilde{b} \leq \tilde{a}$. Furthermore, we introduce the radii $\tilde{R}_1$ and $\tilde{R}_2$ of the (main) curvatures of the gap paraboloid in the coordinate direction indicated by the respective subscript and the magnitude $\tilde{V}$ of the mean sliding velocity. The latter is given by $\tilde{\boldsymbol{V}} = (\tilde{\boldsymbol{V}}_{\rm I} + \tilde{\boldsymbol{V}}_{\rm II})/2$ and has the components $\tilde{V}\cos\chi$, $\tilde{V}\sin\chi$ in the 1- and the 2-direction, respectively, with some positive inclination angle χ ($0 \leq \chi < 2\pi$). Then $\boldsymbol{x}$, the local gap height h, and the time t are appropriately made non-dimensional with, respectively, $\tilde{b}$ (in order to advantageously include the case $\tilde{b}/\tilde{a} \ll 1$ of a highly eccentric contact ellipse in our computational scheme), $\tilde{b}^2/\tilde{R}_2$, and the time $\tilde{b}/\tilde{V}$ representative of the sliding motion.

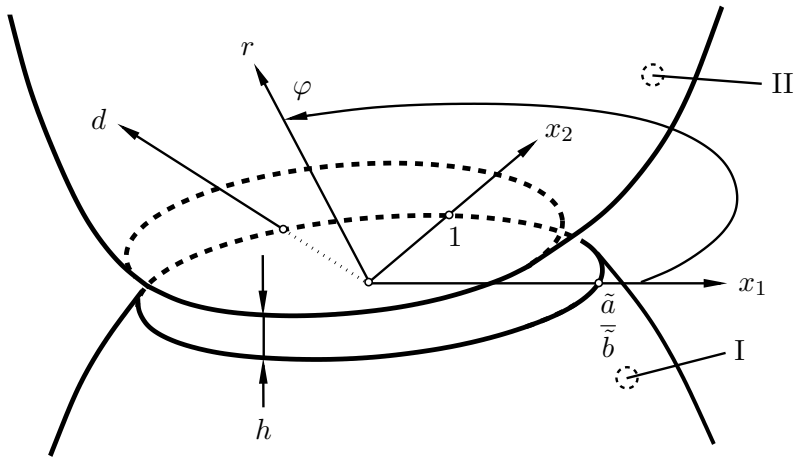

Figure 1: Geometrical configuration (coordinate system attached to body I).

2.1 Homogenisation process

For a small typical distance λ of adjacent surface grooves, characterising the waviness of the rough surfaces and non-dimensional with the reference length, the decomposition

$$h = h_0(\boldsymbol{x}) + A_r(\boldsymbol{x},t)H_r(\boldsymbol{X},t)\,, \tag{1a}$$

$$\boldsymbol{X} = (X_1,X_2) := \big(K_1(\boldsymbol{x})\,x_1, K_2(\boldsymbol{x})\,x_2\big)/\lambda\,,\quad H_r\big(\boldsymbol{X}+(1,1),t\big) \equiv H_r(\boldsymbol{X},t)\,, \tag{1b}$$

invokes the two-scale approach, with λ serving as the micro-scale. Here h_0 represents the sought deformation of the gap height on the macro-scale, merely governed by linearised theory of elasticity (prerequisites in §1). In contrast, the amplitude shape function A_r, the waviness function H_r, and the "wavenumbers" K_1, K_2 account for the corresponding variations of, respectively, the profiles of the roughness elements and the associated fundamental wavelengths in orthogonal directions, thus condensing the information on the asperity distributions on both surfaces involved. Note that the dependence on time reflects the relative motion of the two bodies in contact. The suggested form (1) of the gap height distribution proves sufficiently general as it captures a further separation of scales when undulation, i.e. amplitude and waviness, of the micro-roughness differs strongly on either surface and/or K_1 and K_2 are of distinctly different magnitude on one of the surfaces. Surface texturing, however, could imply more scales.

Let the difference of the pressure in the contact or lubricated regime and the ambient lubricant at sufficiently large values of $|\boldsymbol{x}|$ pressure be non-dimensional with its maximum value $\tilde{p}_H$ obtained from Hertzian contact theory. Furthermore, we introduce the microscopic average saturation θ ($0<\theta\leq 1$), where $\theta=1$ indicates the liquid state and a value $\theta<1$ partial or full vaporisation cavitation the lubricant undergoes when p attains its minimum value given by the cavitation pressure, $p_{0,c}$ (≤ 0). According to (1) and the basic equations describing EHL, these quantities have the asymptotic representations

$$p \sim p_0(\boldsymbol{x}) + \lambda p_1(\boldsymbol{x},\boldsymbol{X},t) + \lambda^2 p_2(\boldsymbol{x},\boldsymbol{X},t) + \cdots\,,\quad \theta \sim \theta_0(\boldsymbol{x},\boldsymbol{X},t) + \cdots \quad \text{as} \quad \lambda\to 0\,. \tag{2}$$

The sole dependence of the leading-order term p_0 on the macro-scale variables $\boldsymbol{x}$ represents a central result of the homogenisation process. Without here being proved rigorously, we see this essentially to ensue from the ellipticity of the lubrication problems assumed to govern p_0 (prerequisites in §1) and p_1. In turn, the resultant leading-order or so-called cell problem of

elasto-hydrodynamic lubrication describes the variation of p_1 on the micro-scale, i.e. with $\boldsymbol{X}$. Here a sufficiently large ratio between the typical roughness wavelength, $\lambda\tilde{b}$, and height of the rather slender gap, $\tilde{b}^2/\tilde{R}_2$, that is

$$1 \gg \lambda \gg \tilde{b}/\tilde{R}_2\,, \tag{3}$$

provides a necessary condition. For the special case of strictly periodic roughness, indicated by constant values of A_r, K_1, K_2, the homogenised problem determining the macroscopic (homogenised) pressure distribution p_0 results in standard manner from averaging the second-order problem governing p_2 over the unit cell $0 \le X_1 \le 1$, $0 \le X_2 \le 1$. Interestingly, only this situation under the assumption of a fully lubricated contact has been tackled so far rigorously by perturbation methods; see e.g. [2]. In view of the representation (1) of h, however, the calculus of Fredholm's alternative provides the proper means for dealing with the elimination of secular terms arising in the second-order problem or, equivalently, the homogenisation process.

However, even for the more general representation (1) of the gap homogenisation is found to be equivalent to averaging. We conveniently set

$$\overline{q}(\boldsymbol{x},t) := \int_0^1 \int_0^1 q(\boldsymbol{x},\boldsymbol{X},t)\,\mathrm{d}X_1\mathrm{d}X_2 \tag{4}$$

for any quantity q and note that $\overline{h} = \overline{h_0} = h_0$ and $\overline{p_0} = p_0$. Also, $h\,\Theta_0(\boldsymbol{x}) := \overline{h\,\theta_0}$ defines the integral (macroscopic) saturation Θ_0 ($0 < \theta \le 1$) at cavitation.

2.2 Governing equations

The pressure induced by viscous effects is described by lubrication theory. As a result of the above considerations and by inserting (2) into the Reynolds equation, the coefficients in these expansions are found to satisfy a hierarchical but strongly interlinked set of modifications of that equation. In particular, the homogenised pressure and saturation in the gap are governed by the solvability condition for the second-order problem that removes the secular terms,

$$\sum\nolimits_{i,j=1}^{2} \frac{\partial}{\partial x_i}\Big(A_{ij}e^{-\alpha p_0}\frac{\partial p_0}{\partial x_j}\Big) = \Gamma \sum\nolimits_{i=1}^{2} \frac{\partial}{\partial x_i}\Big(\Theta_0\big[\cos\chi\, B_{i1} + \sin\chi\, B_{i2}\big]\Big)\,. \tag{5}$$

Herein the viscosity-pressure dependence is modelled specifically in terms of the popular Barus law, $\eta = \exp(\alpha p)$, with α denoting the empirical piezo-viscosity coefficient, non-dimensional with $\tilde{p}_H$, and the dynamic viscosity η of the lubricant, made non-dimensional with an empirical reference value $\tilde{\eta}^*$. From a numerical point of view, this could be accomplished on a more sophisticated level in terms of the Roelands viscosity law, cf. [1], which, however, would not introduce any substantial differences in the analysis. Then it is presumed that the key parameter

$$\Gamma := 12\,\tilde{V}\tilde{\eta}^*\tilde{R}_2^2/\big(\tilde{p}_H\tilde{b}^3\big) \tag{6}$$

controlling the ratio of viscosity-induced to elastic pressure forces, thus the overall surface compliance, is a quantity of $O(1)$. Most important, the homogenisation process results in the flow factors $A_{ij}(\boldsymbol{x})$, $B_{ij}(\boldsymbol{x})$ in (5), whereas the macro-averaged saturation level Θ_0 here does not capture the yet poorly understood phenomenon of micro-cavitation.

For what follows, we assume steady micro-conditions, i.e. we neglect the dependences of H_r and p_1 on t for the sake of a significant reduction of the computational effort but without loosing insight into the basic intricacies of the problem. This simplification is readily confirmed in case of one-sided surface roughness, for instance. Then $p_1(\boldsymbol{x},\boldsymbol{X})$ is conveniently written in the form

$$p_1 = \Gamma\Theta_0\, e^{\alpha p_0}\,\big[\cos\chi\,\Omega_1(\boldsymbol{x},\boldsymbol{X}) + \sin\chi\,\Omega_2(\boldsymbol{x},\boldsymbol{X})\big] + \sum\nolimits_{i=1}^{2} \frac{\partial p_0}{\partial x_i}\,W_i(\boldsymbol{x},\boldsymbol{X})\,. \tag{7}$$

so that the linear leading-order problem in the hierarchy decouples into the four canonical (explicitly parameter-free) periodic unit cell problems

$$\sum\nolimits_{i=1}^{2} \frac{\partial}{\partial X_i}\big[h^3(W_1,\, W_2,\, \Omega_1,\, \Omega_2)\big] = \Big(-\frac{\partial h^3}{\partial X_1},\, -\frac{\partial h^3}{\partial X_2}\,,\, \frac{\partial h}{\partial X_1},\, \frac{\partial h}{\partial X_2}\Big)\,, \tag{8a}$$

$$Q\big(\boldsymbol{x},(X_1,0)\big) \equiv Q\big(\boldsymbol{x},(X_1,1)\big)\,, \quad Q\big(\boldsymbol{x},(0,X_2)\big) \equiv Q\big(\boldsymbol{x},(1,X_2)\big)\,, \tag{8b}$$

$$\frac{\partial Q}{\partial X_2}\big(\boldsymbol{x},(X_1,0_+)\big) \equiv \frac{\partial Q}{\partial X_2}\big(\boldsymbol{x},(X_1,1_+)\big)\,, \quad \frac{\partial Q}{\partial X_1}\big(\boldsymbol{x},(0_+,X_2)\big) \equiv \frac{\partial Q}{\partial X_1}\big(\boldsymbol{x},(1_+,X_2)\big)\,. \tag{8c}$$

Here Q stands for W_1, W_2, Ω_1, Ω_2. Equations (8) govern the small-scale dependences of the functions Ω_i and W_i, $i=1,2$, which for any $\boldsymbol{x}$ fixed implicitly depend on the particular value of $h_0(\boldsymbol{x})$. By (4), then $\overline{\partial Q/\partial X_i} = \partial\overline{Q}/\partial X_i = 0$, $i=1,2$, and the equation governing p_2 is cast into the core problem (5), supplemented with the specific representations of the flow factors

$$A_{ij} = \overline{h^3\delta_{ij} + h^3\,\partial W_j/\partial X_i}\,, \quad B_{ij} = \overline{h\delta_{ij} - h^3\,\partial\Omega_j/\partial X_i}\,, \quad i=1,2\,. \tag{9}$$

Here δ_{ij} denotes the Kronecker symbol. We remark an apparent inconsistency in the counterpart to the formulation (7)–(9) of the cell problems given in [2].

In order to determine both p_0 and h_0, one couples (5) with the well-established expression

$$h_0(\boldsymbol{x}) = h_{00} + \frac{\Lambda\, x_1^2 + x_2^2}{2} + h_{0,e}\,, \quad h_{0,e} := \Pi(\Lambda)\int_{-\infty}^{\infty}\int_{-\infty}^{\infty} \frac{p_0(\xi_1,\xi_2)\,\mathrm{d}\xi_1\mathrm{d}\xi_2}{\sqrt{(x_1-\xi_1)^2+(x_2-\xi_2)^2}}\,, \tag{10}$$

with $h_{0,e}$ resulting from the theory of linear-elastic deformation as expressed by the Boussinesq–Cerruti (BC) integral, which introduces non-locality to the problem. We emphasize that the equal scaling of the x_1- and x_2-coordinates aims at rendering its the kernel symmetric in order to be exploited efficiently in the calculation scheme (see §4). Furthermore, Λ ($0 \le \Lambda \le 1$) denoting the distortion ratio $\tilde{R}_2/\tilde{R}_1$ of the undeformed gap paraboloid represents the geometric key parameter entering the EHL problem, and its eigenvalue h_{00} is due to the compatibility condition

$$\int_{-\infty}^{\infty}\int_{-\infty}^{\infty} p_0(x_1,x_2)\,\mathrm{d}x_1\mathrm{d}x_2 = \frac{2\pi}{3\sqrt{1-e(\Lambda)^2}}\,, \quad e := \sqrt{1-\big(\tilde{b}/\tilde{a}\big)^2}\,. \tag{11}$$

This expresses the equilibrium between pressure forces and the imposed load. The form of the right-hand side of (11), the dependences of both the eccentricity e of the Hertzian contact ellipse and the coefficient Π in (10), as well as the expression of $\tilde{p}_H$ in terms of the physical input parameters result from Hertzian dry-contact theory: see the excursus in §2.3.

Equations (5)–(11) have to be supplemented with the obvious far-field condition

$$p_0 \to 0 \quad \text{as} \quad |\boldsymbol{x}| \to \infty \tag{12}$$

and constraints of Kendahl–Kuhn–Tucker type,

$$h \ge 0\,, \tag{13}$$

$$h_0 \ge 0\,, \tag{14}$$

$$p_0 \ge p_{0,c}: \quad \Theta_0 = 1\,, \quad p_0 = p_{0,c}: \quad 0 < \Theta_0 < 1\,. \tag{15}$$

The restriction (13) is to be coupled with a suitable model of relatively large non-elastic deformation of the single asperities under conditions of dry micro-contact, immediately initiating wear. Concerning the condition (15), the EHL problem represents a free boundary problem in terms of the interface separating the liquid from the cavitated lubricant. An equation of state governing Θ_0 has to be provided if this quantity is expected to drop below the value indicating the transition to full vaporisation of the lubricant. Alternatively, a simpler cavitation model (adopted in §4) suggests to avoid sub-atmospheric pressures by replacing $p_{0,c}$ with 0 and formally setting $\Theta_0 = 1$ throughout. This avoids the subtleties associated with the determination of that interface, where the left-hand side of (5) vanishes so that the equation changes type.

These consideration complete the formulation of the generalised EHL problem for rough concentrated contacts, governed by the input parameters χ, Γ, and Λ and determining the averaged quantities h_0 and p_0.

2.3 Digression on Hertzian theory

The findings of dry-contact theory essential for the present study are condensed in the fundamental relationships (16)–(18) below. For a derivation we refer to [4], pp. 95. At first, e^2 is found to be a strictly monotonically decreasing function of Λ as represented implicitly by

$$K(e^2) - E(e^2) = \Lambda\big[E(e^2)/(1-e^2) - K(e^2)\big]\,, \tag{16}$$

with K and E denoting the complete elliptic integrals of the first and the second kind, respectively (see [3]). Let us note the inverse limiting forms $\Lambda \sim 1 - 3\,e^2/4 + O(e^4)$ as $e^2 \to 0$ (case of axisymmetric contact geometry) and $\Lambda \sim \epsilon[-(\ln\epsilon)/2 + 2\ln 2 - 1] + O[(\epsilon\ln\epsilon)^2]$ as $\epsilon := 1 - e^2 \to 0_+$ (case of an extremely eccentric Hertzian ellipse, pointing to the problem of a line contact). Once e^2 is found numerically for a prescribed value of Λ from (16), $\tilde{a}$ and $\tilde{b}$ are determined by

$$\tilde{a} = \left(\frac{6\tilde{L}\tilde{R}_G}{\pi\tilde{E}^* e^2}\right)^{1/3} \frac{\big[K(e^2) - E(e^2)\big]^{1/3}}{\Lambda^{1/6}}\,, \quad \frac{\tilde{b}}{\tilde{a}} = (1-e^2)^{1/2}\,. \tag{17}$$

Herein $\tilde{L}$, $\tilde{R}_G$, and $\tilde{E}^*$ are the applied load, the Gaussian radius of curvature, $(\tilde{R}_1\tilde{R}_2)^{1/2}$, and the reduced Young's modulus, defined by $2/\tilde{E}^* = (1-\tilde{\nu}_{\rm I}^2)/\tilde{E}_{\rm I} + (1-\tilde{\nu}_{\rm II}^2)/\tilde{E}_{\rm I}$, where $\tilde{E}_{\rm I}$, $\tilde{E}_{\rm II}$ and $\tilde{\nu}_{\rm I}$, $\tilde{\nu}_{\rm II}$ denote the moduli of elasticity and the Poisson's ratios, respectively, of the two bodies. In addition, (11) becomes obvious from the relationship between the Hertzian pressure and the load,

$$\tilde{p}_H = 3\tilde{L}\big/\big(2\pi\tilde{b}\tilde{a}\big)\,. \tag{18}$$

Combining (17) and (18) eliminates $\tilde{L}$. By noting that $\tilde{R}_2/\tilde{R}_G = \Lambda^{1/2}$ and substituting Λ in favour of e^2 by virtue of (16), one finally arrives at

$$\Pi = \frac{\Lambda}{2\pi}\frac{(\tilde{a}/\tilde{b})^2 - 1}{K(e^2) - E(e^2)} = \frac{1}{2\pi}\frac{e^2}{1-e^2}\bigg/\left[\frac{E(e^2)}{1-e^2} - K(e^2)\right]. \tag{19}$$

We find this representation of Π preferable compared to that given in the related study [5] of non-concentric contacts. It is seen that Π assumes finite limits as $e \to 0_+$ and $e \to 1_-$ and $\mathrm{d}\Pi/\mathrm{d}e < 0$ for $0 \le e < 1$. Hence, $\Pi(\Lambda)$ increases strictly monotonically by varying from $\Pi(0) = 1/(2\pi) \doteq 0.15915$ to

$$\Pi(1) = 2/\pi^2 \doteq 0.20264\,, \tag{20}$$

which is the well-known value referring to the classical problem of a (lubricated) circular contact ($e = 0$); see e.g. [2] and, in contrast, [1] for the conventional formulation disregarding surface roughness.

3 ASYMPTOTIC ASPECTS OF THE EHL PROBLEM

A proper numerical treatment of the involved problem posed by (5)–(15) requires the understanding of the far-field variations of p_0 and h_0 to a certain degree of accuracy, provided next. As a cornerstone of the present analysis, we subsequently focus on the behaviour of that system of equations for rather high loads or, equivalently, virtually under Hertzian conditions, here indicated by the limit $\Gamma \to 0$. The assumption $\Lambda \to 0$ (considered above) accounting for the deformation of a lubricated concentrated point to a line contact provides a third limiting case of interest, which deserves a careful analysis but is not tackled here. Remarkably, despite the vital importance of these theoretical aspects for a thorough analysis of the EHL problem of concentrated contacts, neither of them has appreciated adequate attention in the literature so far.

3.1 Far-field analysis

In the limit of large values of $|\boldsymbol{x}|$, the requirement (12) entails vanishing effects of elastic deformation as expressed by the integral term in (10) (which exists for any essentially algebraic decay of p_0). Simultaneously, surface roughness only negligibly affects the widening of the gap: $A_{ii} \sim h_0^3$ and $B_{ii} \sim h_0$ for $i = 1, 2$, and $(A_{12}, A_{21}, B_{12}, B_{21}) \to (0, 0, 0, 0)$ in this limit. To leading order, (5) then reduces to standard form, namely that for an isoviscous lubricant and specifically a parabolic gap separating smooth contacts. Adopting polar coordinates r, φ with $(x_1, x_2) = r(\cos\varphi, \sin\varphi)$, see figure 1, and considering the limit $r \to \infty$ for $0 \leq \varphi \leq 2\pi$, we finally obtain

$$\partial_r\big(r h_\infty^3 \partial_r p_0\big) + r^{-1}\partial_\varphi\big(h_\infty^3 \partial_\varphi p_0\big) \sim \Gamma\big(r\cos(\chi-\varphi)\,\partial_r + \sin(\chi-\varphi)\,\partial_\varphi\big)h_\infty\,, \tag{21}$$

$$h_0 \sim h_\infty := r^2\phi(\varphi)/2\,, \quad \phi(\varphi;\Lambda) := \Lambda\cos^2\varphi + \sin^2\varphi\,. \tag{22}$$

From a computational point of view, it proves sufficient to consider the corresponding leading-order behaviour of p_0 only. (The next stage turns out to account for both the influence of the eigenvalue h_{00} as well as of surface roughness on the flow factors, whereas piezo-viscosity emerges to be significant in still higher-order approximations.)

We accordingly expand $p_0 \sim \Gamma\gamma(r)f(\varphi) + o(\gamma)$ (by omitting any parametric dependences for the sake of clarity) as $r \to \infty$ and seek the at first unknown gauge and (non-trivial) shape functions γ and f, which are assumed to vanish and exhibit periodicity of 2π in φ, respectively. Inserting that representation and (22) into (21) yields the least-degenerate balance

$$\frac{1}{r^2}\frac{\mathrm{d}(r^7\gamma')}{\mathrm{d}r}\phi^3 f + r^3\gamma\frac{\mathrm{d}(\phi^3 f')}{\mathrm{d}\varphi} \sim g(\phi;\chi) := 8\phi\cos(\chi-\varphi) + 4\phi'\sin(\chi-\varphi)\,. \tag{23}$$

Assuming that the forcing term of $O(1)$ on the right-hand side of (23) is negligibly small implies a balance of both terms on its left-hand side and, in turn, a predominantly algebraic decay of γ: $\gamma \sim r^{-\mu}\sigma(r;\mu)$, with some $0 \leq \mu \leq 3$ and some function σ of sub-algebraic variation in r that is essential if $\mu = 0$. The limiting case $\mu = 3$ refers to the remaining possibility, i.e. that both sides of (23) are relevant to leading order we expect to fix the exponent μ. To this end, we study the forced Hill differential equation governing f as resulting from (23),

$$r^{3-\mu}\sigma(r;\mu)\big[\mu(\mu-6)f + 3(\phi'/\phi)f' + f''\big] = U(\mu-3)\,g(\varphi;\chi)/\phi(\varphi;\Lambda)^3\,. \tag{24}$$

Herein $U(x)$ denotes the unit step function with $U(0) = 1$ so that $\sigma(r;3)$ is identified with 1. We first consider the case $\mu < 3$. If Λ is sufficiently close to 1, i.e. $\phi \sim 1$, 2π-periodicity of f is readily dismissed; however, for any $\Lambda \in]0,1[$ it has to be assessed on the basis of Floquet theory, see [6]. One solely infers that the product rather than the value itself of the characteristic multipliers of the homogeneous equation (24) is unity; therefore, no statement about 2π-periodicity of f can be made. However, a more precise conclusion can be drawn from the standard form of (24),

$$\big[\mu(\mu-6) - \omega(\varphi;\Lambda)\big]F + F'' = U(\mu-3)\, r^{\mu-3} g/(\sigma\phi^{3/2})\,, \tag{25a}$$

$$\omega(\varphi;\Lambda) := \frac{3}{4}\frac{\phi'^2}{\phi^2} + \frac{3}{2}\frac{\phi''}{\phi} = \frac{12(1-\Lambda^2)\cos(2\varphi) - 3(1-\Lambda)^2[1+3\cos(4\varphi)]}{8\,\phi^2}\,, \tag{25b}$$

we obtain by setting $F := f\phi^{3/2}$. According to an important result of Floquet theory, the multipliers can be equal to 1 and, simultaneously, f exhibits 2π-periodicity only if the bracketed term in (25a) changes sign for some $\varphi \in [0, 2\pi[$. This in turn is the case as long as $\mu(\mu-6) > \min_{0\le\varphi<2\pi}(\omega) = \omega(\pi/2;\Lambda) = 3(\Lambda-1)$ or, equivalently,

$$\mu < 3 - \sqrt{6+3\Lambda}\,. \tag{26}$$

As the right-hand side of (26) is positive for $0 < \Lambda < 1$, there exists always a dupel (μ, Λ) that satisfies (26). Then the particular values of μ for which f is 2π-periodic have to be specified on the basis of a detailed analytical and accompanying numerical investigation of (25).

For $\mu = 3$ (and $\sigma \equiv 1$) and $0 < \Lambda < 1$ no 2π-periodic homogeneous solution of (25) exists. However, the inhomogeneity in (25a) possibly allows for 2π-periodicity of F, which also has to be confirmed by a more advanced study of (25). Upon substitution of

$$p_0 \sim (\Gamma/r^3) f(\varphi;\Lambda,\chi) \tag{27}$$

in the BC integral, see (10), we have

$$h_{0,e} \sim \Gamma\Pi \int_0^{2\pi} f(\vartheta;\Lambda,\chi)\,\mathrm{d}\vartheta \int_0^{\infty} \frac{\mathrm{d}\rho}{\big[r^2+\rho^2+2r\rho\cos(\vartheta-\varphi)\big]^{3/2}}\,. \tag{28}$$

This can be evaluated further to give

$$h_{0,e} \sim \frac{\Pi\Gamma}{r^2}\,\mathrm{PV}\!\int_0^{2\pi} \frac{f(\vartheta;\Lambda,\chi)}{1+\cos(\varphi-\vartheta)}\,\mathrm{d}\vartheta \tag{29}$$

for the leading-order far-field representation of the elastic contribution to h_0. Specifically, the case $\Lambda = 1$ (26) singles out $\mu = 3$, so that (24) reduces to $f'' - 9f = 8\cos(\varphi-\chi)$ and finally yields

$$f(\varphi;1,\chi) = -(4/5)\cos(\varphi-\chi)\,. \tag{30}$$

By (29) and (20), we finally obtain

$$h_{0,e} \sim -16\Gamma/(5\pi r^2)\cos(\varphi-\chi)\,. \tag{31}$$

Hence, (27) contributes to the overall load as given by (11) only in the presence of cavitation.

It should be noted that the above analysis bears an apparent analogy to the investigation of the pressure in a lubricated concentrated contact near the collapse of the gap. In contrast, there the limiting behaviour $d \to 0$ of the radial distance d from the periphery of the almost elliptic contact region where the contacts are separated by a very thin liquid film is of interest; see figure 1. The pressure near the boundary of the gap then is found to vary predominantly proportional to $d^{-\mu}$ but with $\mu \ge 1$, where one finally again sorts out the extremal case: $\mu = 1$. This behaviour will appear as relevant for the following analysis of highly loaded contacts.

3.2 The heavily-loaded contact problem: a long-standing challenge

As seen from (6) and the analysis in §2.3, Γ decreases as the supplied load $\tilde{L}$ increases and $\tilde{V}$, $\tilde{\eta}^*$, $\tilde{E}^*$ and Λ are kept fixed. More precisely, in case of geometrical similarity, i.e. for a fixed value of e, it reveals a dependence of h_0 on the physical input parameters proportional to

$$\Gamma^{1/2} \propto (\tilde{V}\tilde{\eta}^*)^{1/2}\tilde{E}^{*1/6}\tilde{R}_1^{5/6}/\tilde{L}^{2/3}\,. \tag{32}$$

Finally, $\Gamma \to 0$ as $\tilde{L}$ takes on arbitrarily large values. From this we infer that the interesting case of very high loads is captured by a regular expansion of h_0 and p_0 for small values of Γ as the limit $\Gamma = 0$ describes the case of purely Hertzian contact.

The pressure p_0 admits the Hertzian distribution, $p_{0,H}$, in the limit $\Gamma \to 0$. According to (10) and (14), $p_{0,H}$ is of the well-known elliptic shape, $p_{0,H} = [1 - x_1^2(1-e^2) - x_2^2]^{1/2}$, over the contact ellipse where $h_0 \equiv 0$ and vanishes identically outside, cf. [4]. Next, we assume that the forcing term on the right-hand side of the Reynolds equation (5) can be neglected in this limit, so that $p_{0,H}$ satisfies the homogeneous equation over the contact ellipse subject to a homogeneous Dirichlet boundary condition at its periphery as long as h_0 does not vanish identically inside. However, the elliptic operator governing the left-hand side of (5) then entails the contradiction $p_{0,H} \equiv 0$. We thus arrive at the important result that (5) stays fully intact even for arbitrarily small values of Γ. Inspection of (5) and (10) then gives rise to the expansions

$$\big[h_0/\Gamma^{1/2},\, p_0\big](\boldsymbol{x};\Gamma,\Lambda,\chi) \sim \big[h_{0,H}(\boldsymbol{x};\Lambda,\chi),\, p_{0,H}(\boldsymbol{x};\Lambda)\big] + O\big(\Gamma^{1/2}\big) \quad \text{as} \quad \Gamma \to 0\,, \tag{33}$$

which holds in the region of the Hertzian contact ellipse. The thickness variation $h_{0,H}$ satisfies the rescaled form

$$\sum\nolimits_{i,j=1}^{2} \frac{\partial}{\partial x_i}\Big(A_{H,ij}e^{-\alpha p_{0,H}}\frac{\partial p_{0,H}}{\partial x_j}\Big) = \sum\nolimits_{i=1}^{2} \frac{\partial}{\partial x_i}\Big(\Theta_0\big[\cos\chi\, B_{H,i1} + \sin\chi\, B_{H,i2}\big]\Big)\,. \tag{34}$$

of (5). Most important, here the flow factors involve $h_{H,0}$ as betoken by the subscripts H. Analytical progress is possible for the limiting cases $1-\Lambda \ll 1$ and $\Lambda \ll 1$.

Three findings are important:

(A) expansion (33) answers the celebrated question how the thickness of the lubricant film separating the contacts is scaled correctly in a rational manner;

(B) the thickness variation $h_{0,H}$ is seen as a solution of an inverse lubrication problem as represented by (34), where the pressure term is prescribed by the Hertzian pressure distribution;

(C) the pressure singularity addressed in the last paragraph of §3.2 prevents the emergence of isolated dry regions or starved lubrication in favour of the situation proposed here (unless other physical phenomena not considered so far, as e.g. capillary effects, come into operation).

In view of issue (A), we add that the $\Gamma^{1/2}$-scaling is covered by that in terms of the three Moes dimensionless parameters, see [7], but, to the authors' knowledge, not by the vast amount of its semi-empirical counterparts available in literature, namely by the Hamrock and Dowson, cf. [8], or related parameters; also cf. [1]. Specifically, the dimensional film thickness varies with $\Gamma^{1/2}\tilde{a}^2/\tilde{R}_1$, which by (32) and (17) gives rise to the adequate (Moes) reference height

$$\tilde{h}^* := \big(\tilde{V}\tilde{\eta}^*\tilde{R}_1/\tilde{E}^*\big)^{1/2}\,. \tag{35}$$

This demonstrates that the film thickness becomes essentially independent of the load $\tilde{L}$. The scaling (35) is in good agreement with the aforementioned formulas found in the literature, cf. [1, 8], which also exhibit a rather weak dependences of a characteristic film thickness on $\tilde{L}$. Hence, these are apparently caused by higher-order effects in the expansions (33), not considered in the present study. However, one does not encounter any severe blockage of the lubricant flow through the thin gap when Γ becomes very small, even in the presence of surface roughness. Issue (B) has far-reaching consequences for the proper numerical treatment of the highly loaded case as it gives preference to the intrinsically stable Dowson and Higginson's inverse iterative technique, see [9]. Issue (C) is associated with an asymptotic splitting of the lubricated region: the contact ellipse is confined by a thin annular region having a width d and a thickness of $O(\Gamma^{1/2})$, so that (5) suggests $p_0 = O(d)$ there. This region accounts for the sudden widening of the thin clearance between the contacts. Further away from the ellipse, i.e. for $d = O(1)$, p_0 is small, therefore the gap assumes the shape of the undeformed paraboloid, so that p_0 satisfies (27) for $r \gg 1$ and, in turn, scales with Γ for $r = O(1)$. Finally, matching this outer or the elliptic inner region with the annular region yields $d = O(\Gamma^{1/2})$ for the width of the latter.

4 NUMERICAL INVESTIGATION

The numerical analysis presented is based upon an in some aspects simplified version of the general problem (5)–(15). More general case studies are under way.

4.1 Computational scheme

The equations (5) and (10) and the cell problems (8) are discretised in terms of central finite differences. The latter problem are advantageously solved once for discrete values of h taken from a sufficiently wide range and the resulting flow factors stored in terms of a lookup table. They feed into (5) by means of cubic-B-spline interpolation. The discretisation of the BC-integral yields $\hat{\boldsymbol{h}}_{\boldsymbol{e}} = \hat{\boldsymbol{K}} \cdot \hat{\boldsymbol{p}}$, where $\hat{\boldsymbol{h}}_e$, $\hat{\boldsymbol{p}}$, and $\hat{\boldsymbol{K}}$ are the vectors and the matrix representing the discretisations of $h_{0,e}$, p_0 and the discretised kernel, respectively. We adopt a grid spaced equidistantly in either of the x_1- and the x_2-direction, so that the resulting convolution form of $\hat{\boldsymbol{K}}$ allows for an highly efficient calculation of $\hat{\boldsymbol{h}}_e$ via Fast Fourier Transform. In view of overall computational effort and the analysis in §3.1, this overcompensates the only slightly added accuracy gained by grid adjustment to the rather rapid decay of the solutions for large values of r, which even becomes more pronounced in the interesting case $\Gamma \ll 1$. Furthermore, denotes Δ the typical grid distance, the $O(\Delta^2)$-accuracy of the overall finite-differences scheme is enhanced to $O(\Delta^3)$ by a conventional Richardson extrapolation.

The intrinsic non-local macroscopic coupling between p_0 and $h_{0,e}$, resorting to the microscopic coupling provided by the cell problems (8), suggests the establishment of a direct iterative algorithm such that p_0 and h_0 are calculated via (5) and (10) alternately as the remaining quantity serves as an input. Unfortunately, this is found to be unstable, even by adopting underrelaxation. This has been known for long in the context of smooth-contact problems, where a remedy is given by Dowson's and Higginson's approach of inverse iteration, see [9]. Although desirable, due to the aforementioned coupling applying this technique here represents a hardly surmountable difficulty as h_0 would have to be calculated from the flow factors. As a remaining strategy, the full system of algebraic equations resulting from the discretisation process is solved directly, where an artificial partial suppression of the non-locality of the problem renders the Jacobian a sparse matrix. Adopting $\sqrt{\varepsilon}$ with ε denoting the machine constant, usually of the order 10^{-16}, as the tolerance for convergence is sensible. This turns out to provide a very stable

Physical quantity	Value	Dimension
$\tilde{V}$	0.8	m/s
$\tilde{R} := \tilde{R}_1 = \tilde{R}_2$	1.6×10^{-2}	m
$\tilde{A}_r$	0.1	µm
$\tilde{\nu}_{\rm I} = \tilde{\nu}_{\rm II}$	0.3	–
$\tilde{E}_{\rm I} = \tilde{E}_{\rm II}$	2.05×10^{11}	MPa
$\tilde{E}^*$	2.25×10^{11}	MPa
$\alpha/\tilde{p}_H$	2.2×10^{-8}	Pa^{-1}
$\tilde{\eta}^*$	40.0×10^{-3}	Pa s
$\tilde{L}$	$10 \ldots 100$	N
$\tilde{a} = \tilde{b}$	$1.021 \ldots 2.200 \times 10^{-4}$	m
$A_r = \tilde{A}_r\tilde{R}/\tilde{b}^2$	$0.1534 \ldots 0.03305$	–
$\tilde{p}_H$	$4.577 \ldots 9.862 \times 10^8$	Pa

Table 1: Physical input data for numerical study.

and fast computational scheme, which does not suffer from the tremendous effort and pitfalls associated with the widely-used multi-level/multi-grid techniques proposed in [1]. However, as the method is doomed to fail if the load parameter Γ is quite small, currently including a Gauss–Seidel-type line relaxation modifies the direct approach.

We adopt the simplified cavitation model, see (15), where $p_{0,c} := 0$. In view of (13), wear and, consequently, flattening of the surface roughness elements is modelled in terms of simply trimming them, namely "cutting" the particular asperity spikes at the critical locations $\boldsymbol{x}$ where (13) would be violated otherwise. Here (13) is relaxed in order to avoid dry isolated regions at the micro-scale by bounding h from below by 10^{-8}, which reasonably compares with $\sqrt{\varepsilon}$. See also the respective comments on those issues at the end of §2.2.

4.2 Case study

In order to allow for a detailed comparison of results referring to two configurations which are identical unless the second takes into account (one-sided) surface roughness, we identify the first with the benchmark problem of a concentric contact considered in [1], pp. 195, where no homogenisation is required. The physical input data used in the present study only differ by a slight difference in the values of $\tilde{E}^*$. Specifically, the load $\tilde{L}$ varies from 10 to 100 N. The movement shall be just in positive x_2-direction, i.e. $\chi = \pi/2$, and we assume strictly periodic and uni-directional roughness, specified in the form, cf. (1),

$$H_r = \sin(2\pi X_2) + 0.5\sin(7\pi X_2)\,. \tag{36}$$

Since H_r is non-smooth with respect to its 2π-periodicity, (36) models sharp roughness peaks encountered for $X_2 = 0$ and 1. Here the asperity spikes representative of two-dimensional roughness patterns are replaced by ridges, aligned with the x_1-direction. As a consequence, $\partial(\Omega_1, \Omega_2)/\partial X_1 \equiv (0, 0)$, so that on the right-hand side (5) only B_{22} is in operation. Therefore, the problem is symmetric with respect to the x_2-axis. The value of the dimensional maximum surface roughness, $\tilde{A}_r$, refers to a realistic engineering surface, thus giving rather small values of A_r. The input data are summarised in table 1, where for those depending on the variable load $\tilde{L}$ the corresponding bounds are given with suitable accuracy.

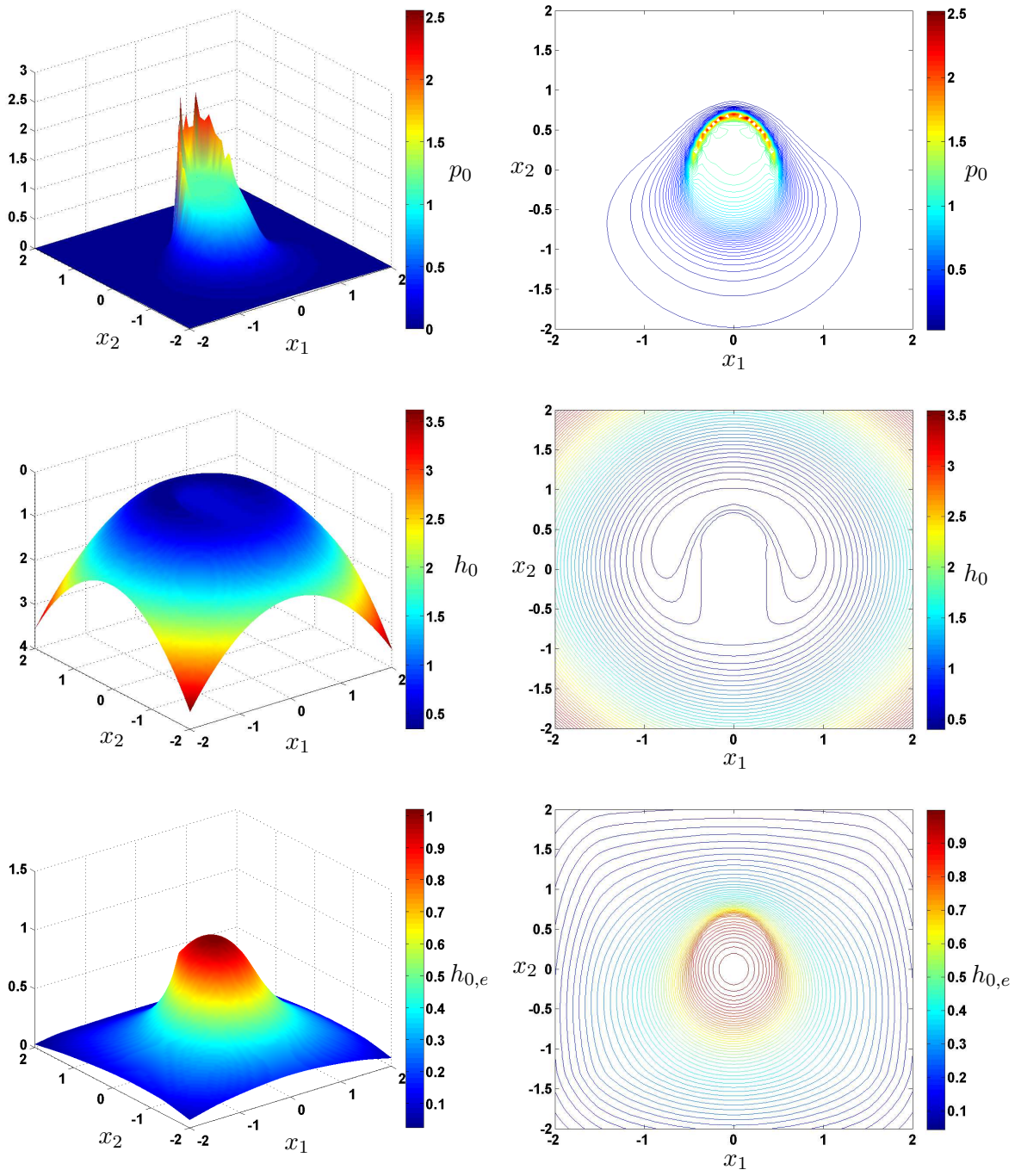

Figure 2: Case $\tilde{L} = 10\,\mathrm{N}$, $\Gamma \doteq 0.2016$: p_0, h_0, $h_{0,e}$.

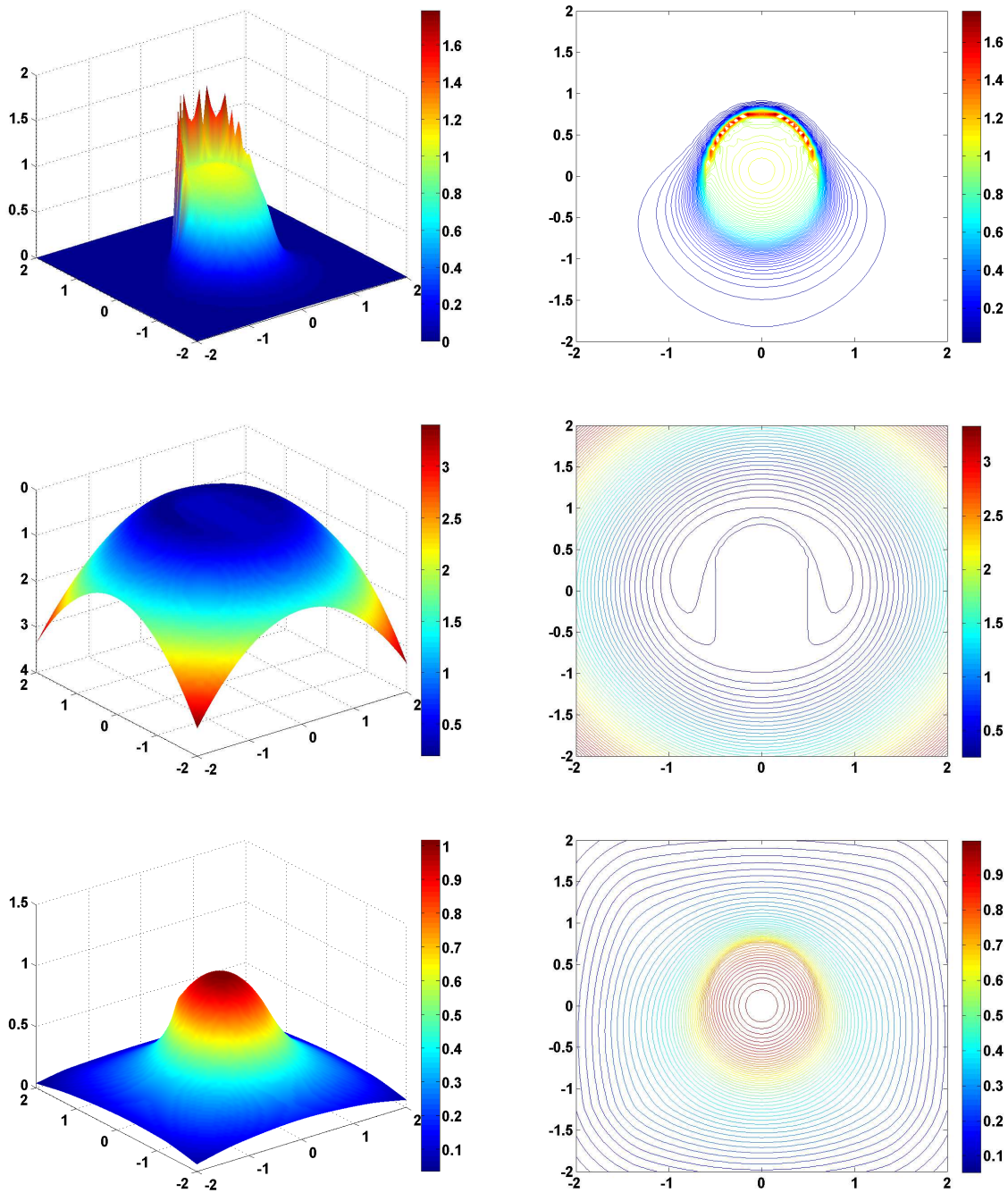

Figure 3: Case $\tilde{L} = 20\,\mathrm{N}$, $\Gamma \doteq 0.0800$: p_0 h_0, $h_{0,e}$ (alignment and legend as in figure 2).

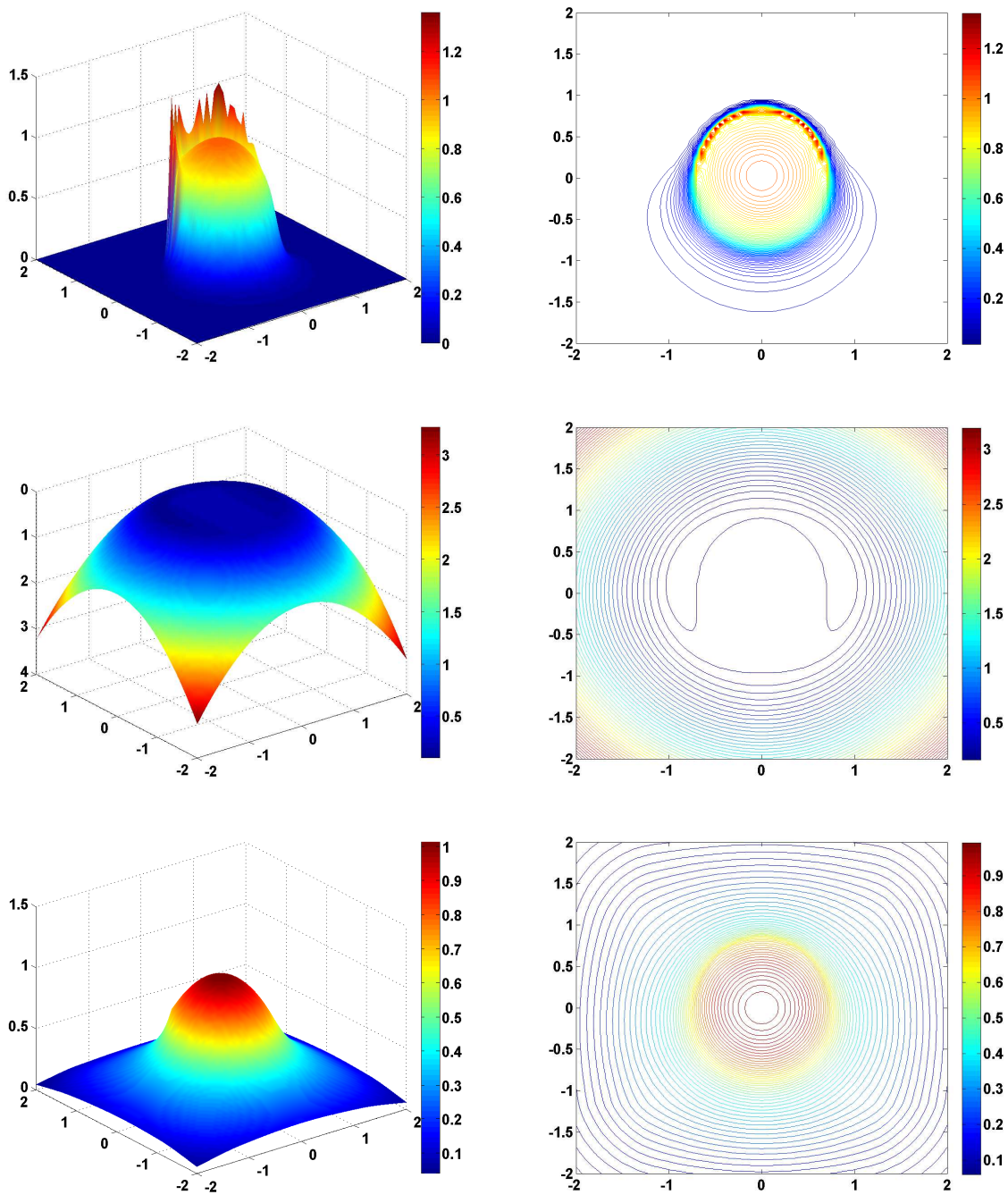

Figure 4: Case $\tilde{L} = 40\,\mathrm{N}$, $\Gamma \doteq 0.0317$): p_0 h_0, $h_{0,e}$ (alignment and legend as in figure 2).

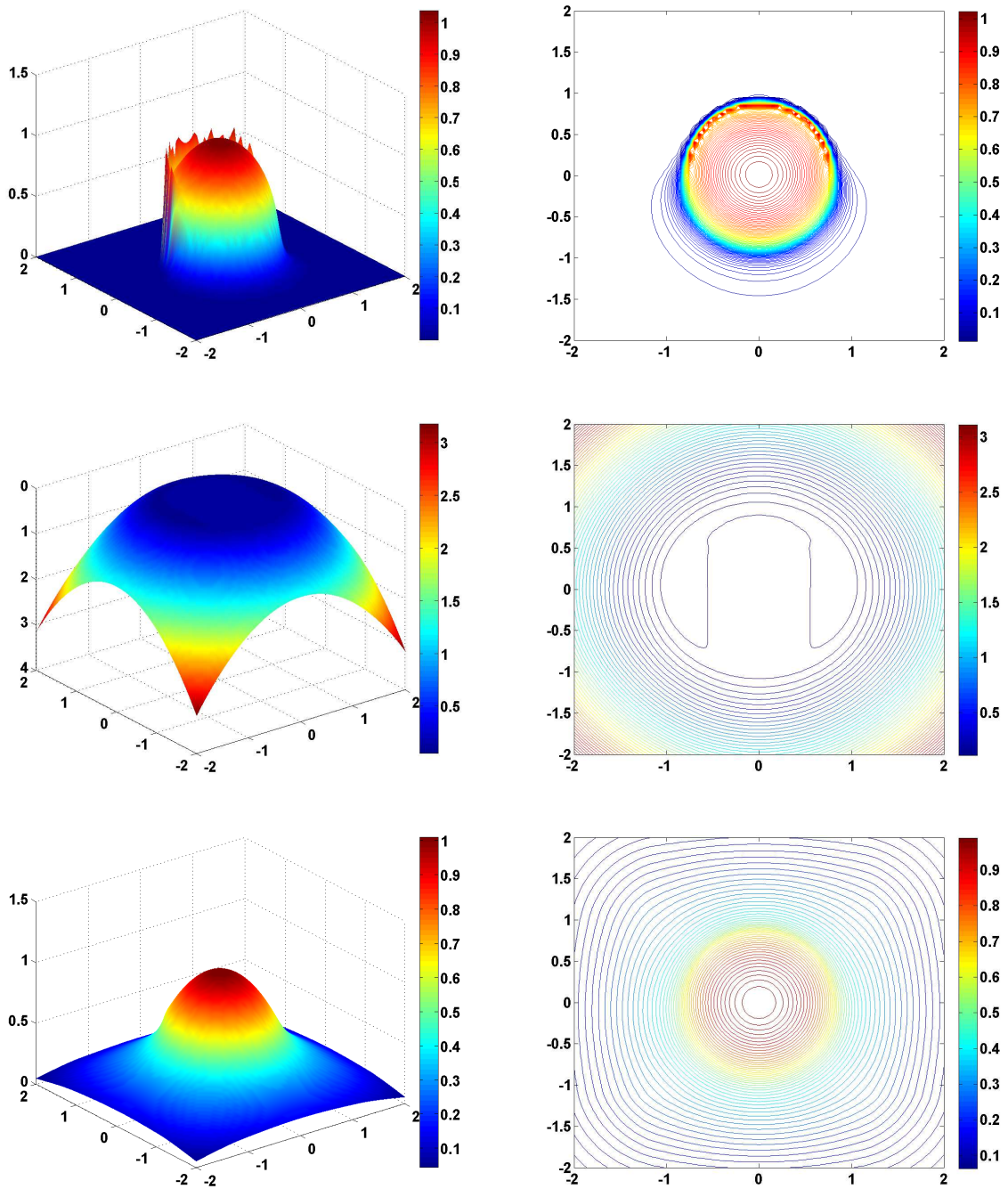

Figure 5: Case $\tilde{L} = 80\,\mathrm{N}$, $\Gamma \doteq 0.0126$: p_0, h_0, $h_{0,e}$ (alignment and legend as in figure 2).

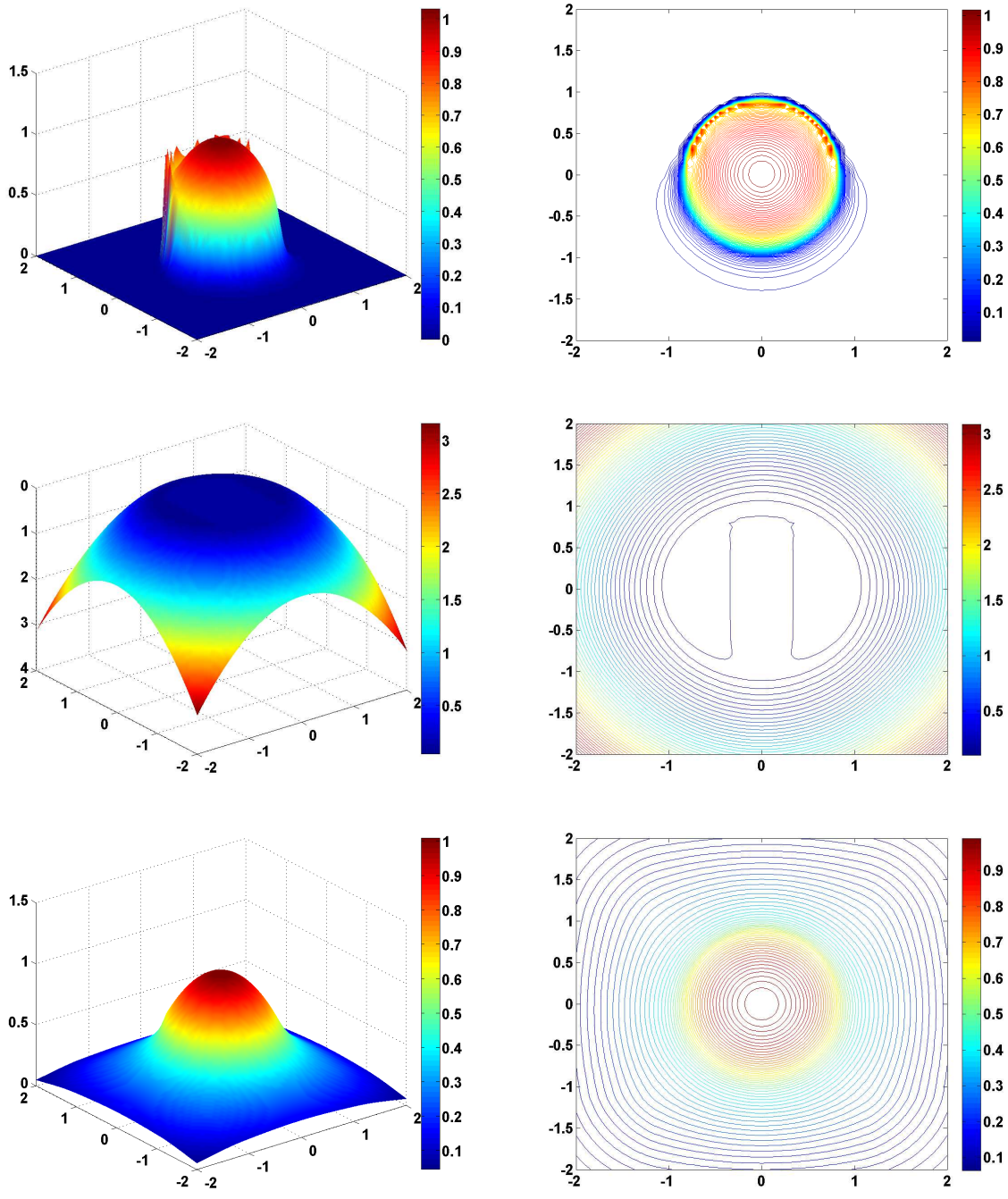

Figure 6: Case $\tilde{L} = 100\,\mathrm{N}$, $\Gamma \doteq 0.00936$: p_0, h_0, $h_{0,e}$ (alignment and legend as in figure 2).

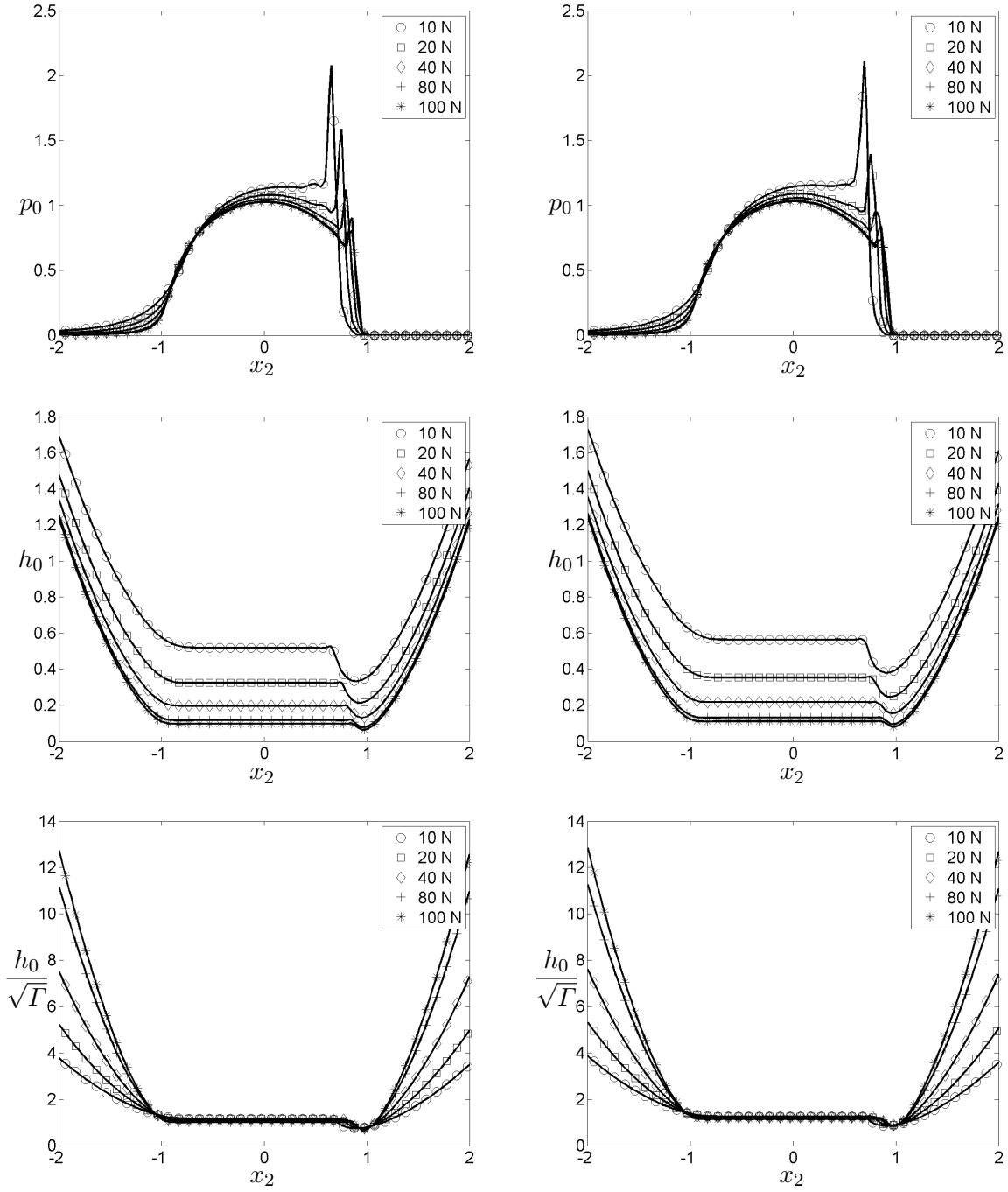

Figure 7: Comparison between results for smooth (*left*) and rough (*right*) surfaces evaluated at the line of symmetry ($x_1 = 0$), data points (*symbols*, distinguishing the loads) interpolated by cubic splines (*solid*). Note the agreement with the scaling predicted by (33).

Note that $\Lambda = 1$, so that Π is given by (20) and (27) applies for $r \gg 1$. This behaviour is conveniently prescribed in the form $\partial_r p_0 = -3p_0/r$ at the boundary of the computational domain. Restricting the latter to the rather small square $-2 \leq x_1 \leq 2$, $-2 \leq x_2 \leq 2$ enclosing the unit circle of Hertzian contact then proves sufficient.

First numerical solutions of the EHL problem are encouraging. In the present study the focus lies on the variation of the parameter Γ, controlled by the values of $\tilde{L}$, where we want to exhaust our numerical method by allowing Γ to take on values as small as possible. The results are displayed in figures 2–6. The characteristic "horseshoe-pattern" of the isolevels are clearly visible and disappear for rather large loads. Notwithstanding the rather small amplitude A_r of the surface roughness, comparatively considerable differences between the results and the reference data referring to smooth surfaces are detected, at least partially: see figure 7. As general statement, the scaling put forward by (33) applies perfectly to either case even for moderate values of Γ, whereas both p_0 and h_0 are slightly increased in the rough-contact case. This sensitiveness is also recognised by the spurious oscillatory behaviour of the pressure peaks characteristic of the leading edge of contact, which requires a finer grid resolution in subsequent studies. However, when the load is increased the pressure precursor becomes more narrow and thus more difficult to resolve as the Hertzian pressure distribution $p_{0,H}$ crystallizes. Finally, this "'spiky crest" in the pressure distributions vanishes as $p_0 \to p_{0,H}$ for $\Gamma \to 0$. Tied in with this phenomenon as h_0 becomes very small, the problem is expected to give rise to serious convergence problems when the load exceeds values definitely larger than $100\,\mathrm{N}$. On the other hand, for the time being the macro-scale is resolved by 81 grid points at the maximum in both the x_1- and the x_2-direction. Then the truncation error of $O(\Delta^3)$ is numerically of the order 10^{-4}, which provides a lower bound for the numerical magnitude of h_0. Therefore, in view of the results obtained for $\tilde{L} = 100\,\mathrm{N}$, the solutions are reliable as h_0 takes on values of about 0.0977 and 0.1108 for $r = 0$ and attains its minima where $h_0 \doteq 0.0404$ and 0.0446 for $(x_1, x_2) \doteq (\pm 0.9, 0.25)$ and $(x_1, x_2) \doteq (\pm 0.9, 0.2)$ in the case of the smooth and the rough contacts, respectively. Nonetheless, an efficient resolution for very low values of Γ should advantageously take into account the asymptotic structure of the problem elucidated in §3.2, despite the aforementioned undeniable difficulties associated with the solution of (34) in terms of $h_{0,H}$.

In addition, the behaviours for large values of r put forward by (27), (30), and (31) are confirmed satisfactorily well by the numerical findings, even for moderate values of r, i.e. not too far outside the Hertzian contact ellipse. Specifically, their agreement with the radial dependences of p_0 and $h_{0,e}$ is excellent, as seen from the log–log plots in figure 8. Here the variations of $h_{0,e}$ and p_0 in the $45°$-trailing direction, i.e. for $\varphi = -\pi/4$, are compared for the case $\tilde{L} = 10\,\mathrm{N}$. From the dominant asymptotic representations (27) and (31) one infers the fits $\lg(p_0, h_{0,e}) \sim -(3,2)\lg r + (c_p, c_h)$ with $c_p = \lg(\sqrt{2}\Gamma/5) \doteq -1.244$ and $c_h = \lg[4\sqrt{2}\Gamma/(5\pi)]$ $\doteq -1.140$, whereas the least-squares fits $\lg p_0 \approx -3.20\lg r - 1.70$, $\lg h_{0,e} \approx -1.90\lg r - 0.16$ rely on the entire computational domain, i.e. on the interval $1.06\ldots < r \leq \sqrt{8.0} \doteq 2.828$. One observes a more pronounced impact of disregarded higher-order effects on the decay of $h_{0,e}$.

5 CONCLUSIONS

An attempt has been made to rigorously extend the classical description of non-conformal concentrated contacts under the action of elasto-hydrodynamic lubrication by including all the physical mechanisms associated with surface roughness in form of a quite general formulation of the problem. Here the most intriguing phenomena of interest include cavitation, wear due to non-elastic deformation of the asperities, and their interplay with piezo-viscous effects.

The asymptotic approach exploits the underlying separation of length scales by virtue of a

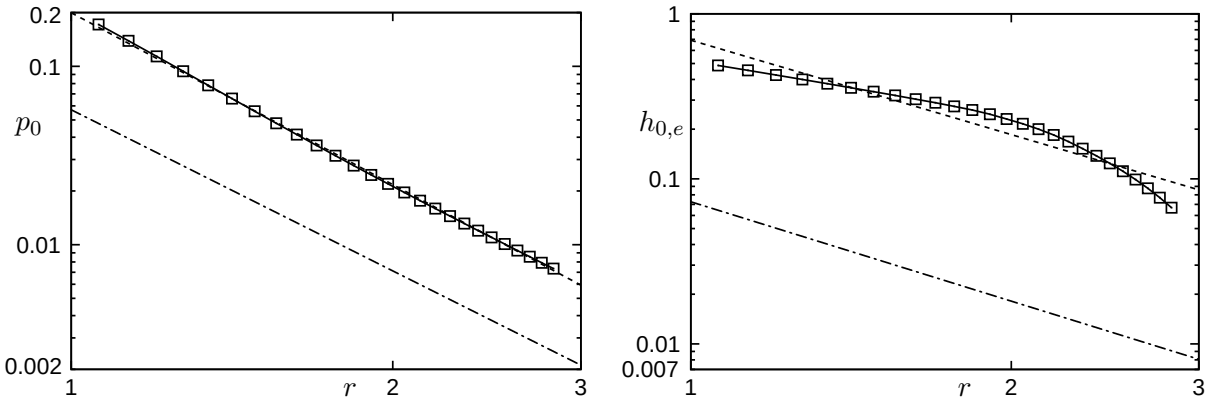

Figure 8: Decay of p_0 and $h_{0,e}$, data points (*squares*) interpolated by cubic splines (*solid*) versus linear least-squares (*dashed*) and asymptotic regressions (*dash–dotted*).

homogenisation process, which finally leads to a hierarchical but coupled system of (nonlinear) partial integro-differential equations that account for all the effects at play in a rational manner. Specifically, the limiting case of relatively high loads is scrutinised. First numerical results allow for assessing the deviations of the typical "horseshoe-type" homogenised distributions of the contact pressure as well as the height of the lubricated gap from those referring to smooth solid contact surfaces. Most important, a preliminary answer is given to the long-standing question of the average thickness of the very thin liquid film separating the contacts. Here more intensified analytical and numerical effort seems expedient. As a remarkable finding, the film thickness is found to be essentially independent of the imposed load, which avoids a severe blockage of the lubricant flow even in case of distinctive surface roughness. Regarding the latter, devising a technique related to Dowson's and Higginson's inverse method represents a desirable though very challenging task.

In particular, it is found that the pressure singularity inevitably emerging at the periphery of dry isolated contact areas under the conventional assumptions of elasto-hydrodynamic lubrication severely hampers their computational prediction. Amongst other topics, this phenomenon of starved lubrication together with its counterpart on the micro-scale and the accompanying occurrence of micro-cavitation are topics of the current research activities. Future efforts will also focus on the inclusion of inertial effects on the scale of the roughness, i.e. for asperity elements which are not so slender such that the lubrication approximation no longer applies to the bypassing flow.

ACKNOWLEDGEMENTS

The authors are greatly indebted to the Austrian Research Promotion Agency (FFG) for granting this research within the framework of the COMET K2 Excellence Center of Tribology (*XTribology*).

REFERENCES

[1] C.H. Venner, A.A. Lubrecht: Multi-level methods in lubrication. *Tribology Series* 37, ed. D. Dowson, Elsevier, 2000.

[2] G. Bayada, S. Martin, C. Vázquez: Micro-roughness effects in (elasto)hydrodynamic

lubrication including mass-flow preserving cavitation model. *Tribology International*, 39(12) (2006), 1707–1718.

[3] M. Abramowitz, I.A. Stegun (eds.): Handbook of mathematical functions with formulas, graphs, and mathematical tables. Dover Publications, 1972.

[4] K.L. Johnson: Contact mechanics. Cambridge University Press, 1987.

[5] C.H. Venner, A.A. Lubrecht: Revisiting film thickness in slender elasto-hydrodynamically lubricated contacts. Special Issue Paper. *Proc. IMechE Part C: J. Mechanical Engineering Sciences*, 224(12) (2010), 2549–2558.

[6] W. Magnus, S. Winkler: Hill's equation. Interscience Publishers (John Wiley & Sons), 1966.

[7] H. Moes: Optimum similarity analysis, an application to elastohydrodynamic lubrication. *Wear*, 159(1) (1992), 57–66.

[8] B.J. Hamrock, D. Dowson: Ball bearing lubrication, the elastohydrodynamics of elliptical contacts. John Wiley & Sons, 1981.

[9] D. Dowson, G.R. Higginson: A numerical solution to the elasto-hydrodynamic problem. *J. Mechanical Engineering Sciences*, 1(1) (1959), 6–15.